ABSTRACT

Title of Document: WIND-DRIVEN PLUME DISPERSION NEAR A BUILDING

Young Ern Ling, Master of Science, 2008

Directed By: Associate Professor André W. Marshall, Department of Fire Protection Engineering

The dispersions of smoke or hazardous materials during accidental releases are of concern in many practical applications. A technique combining salt-water modeling and Particle Image Velocimetry (PIV) is developed to study the dispersion of a buoyant plume in a complex configuration. Salt-water modeling based on the analogy between salt-water flow and fire induced flow has proven to be a successful method for the qualitative analysis of fire induced plumes. With the use of non-intrusive laser diagnostics such as the PIV, detailed measurements of the velocity field can be taken for quantitative analysis of the plume behavior. The technique is first validated for a canonical unconfined plume scenario by comparing the results with theory and previous experimental data, and subsequently extended to qualitatively and quantitatively analyze plume dispersion in a crossflow with the construction of a crossflow generation system for the salt-water modeling facility. Lastly, plume dispersion in a crossflow near a building is analyzed.

WIND-DRIVEN PLUME DISPERSION NEAR A BUILDING

By

Young Ern Ling

Thesis submitted to the Faculty of the Graduate School of the
University of Maryland, College Park, in partial fulfillment
of the requirements for the degree of
Master of Science
2008

Advisory Committee:
Associate Professor André W. Marshall, Chair
Professor Marino di Marzo
Associate Professor Arnaud Trouvé

Acknowledgements

My sincere appreciation goes to the Singapore Civil Defence Force for sponsoring me in this MS program, as well as the Fulbright Program for making this experience of educational and cultural exchange possible.

I cannot thank Professor Andre W. Marshall enough for being my advisor, and for his guidance and motivation throughout the entire course of the research. Without his resourcefulness, all this would not have been possible. Many thanks to Professor Marino di Marzo and Associate Professor Arnaud Trouvé for their time, support and advice in the advisory committee, and Professor James G. Quintiere, Associate Professor James A. Milke and Assistant Professor Peter B. Sunderland for imparting their knowledge in various subjects of fire protection engineering.

I am grateful to Dr Xiaobo Yao for freely sharing his expertise and knowledge in all aspects of conducting the salt-water experiments. Special thanks to Mr Fernando Raffan for imparting his skills on use of the PIV system, and to my colleagues, Mr Carlos Cruz, Mr Ren Ning, Miss Shirley Luo and Mr Adam Goodman for their assistance in one way or another in the project. I am also especially grateful to Mary Lou Holt and Sharon Hodgson who have always promptly helped me in acquiring the items that I need for the project.

My deepest heartfelt gratitude goes to my wife and best friend, Shi-Wei, who has sacrificed beyond measure to provide me with unwavering support and help. Thank you for Jeremy and Carissa, for always being there, and for loving me all the time.

Most of all, thanks be to God for His providence and goodness.

Table of Contents

List of Tables

List of Figures

Nomenclature

B specific buoyancy flux

B' modified buoyancy flux,

D^* characteristic length scale, $D^* = \left(\frac{\beta_{sw} \dot{m}}{\rho_0 g^{1/2}} \right)^{2/5}$

d_p diameter of seeding particle

d_i diameter of seeding particle image on CCD chip

d_{diff} diffraction limited image diameter

$f_\#$ f number of lens system

g gravitational acceleration

H building height or height above source

L_b source distance from building

L characteristic length scale

M magnification of optical system

$\dot{Q}$ heat release rate

Q^* dimensionless source strength for fire, $Q^* = \beta_T \dot{Q} / \rho_0 c_p g^{1/2} x_3^{5/2}$

Re Reynolds number

$\dot{m}_{salt}$ salt release rate

m_{sw}^* dimensionless source strength for salt water, $m_{sw}^* = \beta_{sw} \dot{m}_{salt} / \rho_0 g^{1/2} x_3^{5/2}$

U_{CF} crossflow velocity

U_{plume} centerline velocity of plume along trajectory

u_i plume mean velocity

u_i^* dimensionless velocity, $= u_i (gH)^{-1/2} (Q^*)^{-1/3}$ or $= u_i (gH)^{-1/2} (m_{sw}^*)^{-1/3}$

$\dot{V}_o$ source volumetric flow rate

W width of building

x_s^* characteristic vertical distance for steady plume in crossflow

z_o virtual origin

Y_{salt} salt mass fraction

Greek

β volumetric expansion coefficient, = $1/T_0$ for fire; = 0.76 for salt water

ρ_o source fluid density

ρ_∞ ambient fluid density

Subscript

c centerline

sw salt water

T fire

inj injector position

o source value or virtual origin location

∞ ambient value

Chapter 1: Introduction

Airborne releases and dispersion of smoke plumes or other hazardous agents have been a principal concern of communities and emergency managers. Communities including public health officials, state and regional poison centers, hospitals, and non-governmental organizations that provide care and shelter for affected populations have always prepared themselves to deal with accidental releases from industrial sites, energy facilities, and vehicles transporting hazardous materials. The public has become more and more aware of the harmful effects of accidental releases through major accidents and events such as the use of CB agents in World Wars I and II, the nuclear tests of the 1950s, the 1968 Clean Air Act and its 1990 amendments passed by the U.S. Congress, the discovery of acid lakes in the 1970s, the discovery of the ozone hole in the 1980s, the Bhopal chemical accident, the Chernobyl nuclear plant accident, the Gulf war, the Japanese subway chemical agent release, the September 11 terrorist attacks and the Buncefield Oil Depot fires in the UK. As such, there has always been a propelling force for research in the area of transport and dispersion of pollutants in the atmosphere.

1.1 Motivation

Accidental releases from industrial processes mishaps, explosions and unwanted fires often result in the release of unconfined, buoyant turbulent plumes of smoke or other hazardous materials. Such plumes are most likely to be dispersed by wind in the atmosphere, carrying the toxic or undesirable effects of the plume to surrounding areas. On a large scale, plumes may be dispersed as far as tens of

kilometers from the source of release. The study of wind-driven plume dispersion will provide data and knowledge for evaluating the many methods of plume predictions that have been developed, contributing substantively in practical applications from preparation and planning for possible future events, to emergency response in the minutes to hours after an event occurs, and to the post-event recovery and analysis.

Fire induced flows have been extensively studied using various methods, amongst which is the salt-water modeling technique. In previous studies, salt-water modeling has been effectively used to visualize the dispersion of smoke in different flow configurations with the aid of a tracer dye introduced into the salt-water source. Combined with laser diagnostics such as the Planar Laser Induced Florescence (PLIF) Laser Doppler Velocimetry (LDV), or Particle Image Velocimetry (PIV) methods, the qualitative salt-water modeling technique has been successfully used to quantitatively characterize the dispersion of buoyant plumes and fire induced flow transport along ceilings. Keeping in mind the practical applications on predicting plume behavior in accidental releases, the salt-water modeling technique is extended to analyze the dispersion of unconfined, buoyant plumes in a complex environment.

1.1 Literature Review

1.1.1 Previous Work on Plume Dispersion

Recognizing the potential consequences of air pollution, studies on plume dispersion in a crosswind began as early as the 1900s to investigate the effects of releases from smoke stacks of power plant buildings. Turbulent jets were released into quiescent or crossflow air streams in wind tunnels by researchers such as

Sherlock and Stalker [1], Hohenleiten and Wolf [2], and Bryant [3] who understood the importance of exhaust to free stream velocity ratio, but did not place emphasis on density ratio, Reynolds number, Froude number, or momentum flux ratios. These studies were able to describe the flow structures such as bifurcation in the crossflow, von Karman vortices, entrainment and downwash near a building and the broadening effects of wake turbulence on the downwind plume. Experimentalists at that time agree that similarity in wind profiles including turbulent behavior, a fully turbulent exhaust jet, equality of density, momentum and buoyancy ratios are necessary to simulate plume trajectory and mixing behavior correctly in the laboratory. Strom and Halitsky [4], Halitsky [5, 6, 7], Cermak et al. [8] and Melbourne [9] were among the first to address such simulation criteria for air pollution aerodynamics study. However, simulation of the buoyancy parameter or the Froude number at reasonable wind tunnel scales implies often resulted in low model wind speeds with poor turbulent similarity. Though many proposals have been made to determine a set of acceptable simulation criteria, they are not always consistent due to the distorted scaling of density, stack diameter and exhaust velocities, and it was not until Snyder [10, 11] whose suggestions are most accepted as the standard simulation criteria.

Golden [12] proposed a minimum building Reynolds number criterion for building emission studies above which near-building concentration distributions would be flow independent. He concluded one should maintain $Re = U_{CF} H / \nu$ > 11,000 where U_{CF} was approach speed at building height H. The work by Castro and Robins [13] and Snyder [14] have further shown that the *Re* criterion is affected by source location, building orientation, and measurement location.

One of the major contributors to research in atmospheric dispersion in the late 1960s into the early 1970s is Briggs who published his first plume rise model observations and comparisons in 1965 [15]. In 1968, at a symposium sponsored by CONCAWE (a Dutch organization), he compared many of the plume rise models then available in the literature [16]. In that same year, Briggs also wrote the section of the publication edited by Slade [17] dealing with the comparative analyses of plume rise models. That was followed in 1969 by his classic critical review of the entire plume rise literature [18], in which he proposed a set of plume rise equations which have since become widely known as "the Briggs equations". Subsequently, Briggs modified his 1969 plume rise equations in 1971 and in 1972 [19, 20]. Briggs' equations for bent-over, hot buoyant plumes have become widely known and widely used in many dispersion models up till today. The equations are based on observations and data involving plumes from typical combustion sources such as the flue gas stacks from steam-generating boilers burning fossil fuels in large power plants. The stack exit velocities were in the range of 6 to 30 m/s with exit temperatures in the range of 120 to 260 °C.

Another classical analytical method developed to characterize plume dispersion in a crosswind is the Gaussian plume model which focuses on a time-average plume that varies smoothly in space. Analytical Gaussian plume models assume that the concentration of the agent downwind of the source (averaged over a large number of realizations of the given dispersion problem) has the form of the Gaussian, or "normal", probability distribution in the vertical and lateral directions. The amplitude and width of this "bell curve" are determined analytically by the rate

of emission, mean wind speed and direction, atmospheric stability, release height, and distance from the release. Such models assume continuous and constant emission of agent, and they also generally assume flat terrain, no chemical reactions or absorption, and constant mean wind speed and direction with time and height. Gaussian plume models for continuous releases are the oldest and simplest examples of ensemble-average dispersion models. They require a minimum of input information such as the average wind speed and direction, including rudimentary information on whether the wind and temperature conditions favor turbulence and hence mixing, which allows for the diagnosis of the downstream growth of the Gaussian plume.

Boundary layer meteorological wind tunnels were extensively used to study point, line, area, and volume sources in the 1970s by Cermak [21]. A good number of studies on round turbulent unconfined nonbuoyant and buoyant flows were also done by Turner [22, 23], Tennekes and Lumley [24], Hinze [25], Chen and Rodi [26] and List [27]. The penetration properties of plumes were also analyzed by Morton [28], Middleton [29], and Delichatsios [30]. As most practical flows are exposed to crossflow, results obtained from still fluids studies were extended to corresponding round turbulent buoyant sources in crossflow by Anwar [31], Lutti and Brzustowski [32], Andreopoulos [33], Alton et al. [34], and Baum et al. [35].

1.1.2 Salt-Water Modeling and Fire Plumes

Predicting smoke and flame behavior can be based on full-scale field experience, zone modeling using analytic integral approximations that capture the gross flow behavior, fine-scale numerical modeling or physical modeling at reduced scale. Froude modeling (*Fr*) using either air or saltwater is probably the most common kind of physical modeling for hot smoke transport by simulating a full-scale fire induced flow with a turbulent buoyancy driven flow in a geometrically similar small-scale configuration. Quintiere [36] provides a variety of examples of how physical modeling has been used to model various aspects of fires including: simple fire plumes, ceiling jets, burning (pyrolysis) rate, flame spread, and enclosure fires. Heskestad [37] includes cases of sprinklered fires. Sangaras and Faeth [38] used salt-water modeling to analyze the temporal development of round turbulent non-buoyant starting jets and buoyant starting plumes theoretically and experimentally by observing the motion of the dye tracer. Steckler et al. [39] established the fire/salt-water analogy through quantitative scale analysis and salt-water flow visualization experiments with a scale multi-compartment warship. Kelly [40] compared dimensionless event times between salt-water experiments and computational fluid dynamics (CFD) analysis of fires in geometrically similar multi-room compartments and found quantitative agreement. Clement and Fleischman [41] also compared salt-water experiments in a two-room enclosure with CFD analysis using the Fire Dynamics Simulator (FDS). More recently, Jankiewicz [42] combined salt-water modeling and the Planar Laser Induced Fluorescence (PLIF) technique to explore the applicability of these techniques to the prediction of detector response times. He

found excellent agreement between dimensionless front arrival times in the salt-water model and the full-scale fire experiments. Excellent quantitative agreement between PLIF salt-water measurements and fire plume measurements have been demonstrated by Yao et al. [43, 44, 45] in the unconfined plume and impinging plume configurations, who compared scaled salt-water measurements with McCaffrey's fire plume centerline temperature measurements, point source plume theory [46], and Alpert's ceiling jet analysis [47].

The salt-water modeling and flow visualization technique has been used by Sangras et al. [48] to investigate the self-preserving properties of round turbulent thermals, puffs, starting jets and starting plumes in uniform and still fluids in still environment. Soon after, Diez et al. [49] extended the work of Sangras et al. to study similar flows in an unstratified uniform crossflow experimentally. They measured the vertical, horizontal and radial penetration properties of the flows as a function of time for various source conditions, and formulated the self-preserving scaling relationships for the flows and used the experimental measurements to evaluate the effectiveness of their scaling relationships and to determine the empirical parameters within the scaling laws.

1.2 Research Objectives

The purpose of this research is to develop an experimental technique using salt-water modeling and Particle Image Velocimetry (PIV) diagnostics to characterize plume dispersion in a crossflow. The technique will be applied to an unconfined buoyant plume to provide quantitative measurements of the velocity field in the

plume. The data obtained will be compared with results obtained using PLIF and LDV techniques in past experiments. Building on the existing salt-water facility, a crossflow generation system will be developed to simulate a crosswind in the fresh water tank. Plume dispersion in a crossflow will then be quantitatively and qualitatively analyzed using the same technique. Subsequently, the technique will be extended to study an unconfined mixed convection problem in a complex environment involving a crosswind and structures such as a building.

The specific objectives of this research are to:

- Validate the PIV diagnostic technique with salt-water modeling using a classical unconfined buoyant plume configuration by comparing the quantitative measurements with past experimental data and theory.

- Develop and characterize a crossflow generation system for the analysis of wind-driven plume dispersion using the salt-water modeling technique.

- Analyze qualitatively and quantitatively the dispersion of a buoyant plume in crossflow by comparing the trajectory and velocity measurements with experimental data and theory.

- Analyze qualitatively and quantitatively the dispersion of a buoyant plume in a crosswind near a building.

Chapter 2: Approach

The concept of the fire/salt-water analogy is first discussed, followed by the application of the analogy to dispersion behavior in a complex configuration. Important parameters and dimensionless quantities that capture the essential features of the physics governing the dispersion of a buoyant plume in crossflow are highlighted and the scaling laws are presented. Details of the test facility and the diagnostic tools used in the experiments are described. The experimental methodology is then explained, leading to the discussion of the results in the next chapter.

2.1 Fire/Salt-Water Analogy

The theoretical basis of salt-water modeling is a mathematical analogy between fire induced and salt-water flows. Mathematical equations governing the fire induced and salt-water flows are first formulated separately. Appropriate non-dimensionalizing factors are then chosen to reduce the two mathematical treatments to precisely the same form, forming the fire/salt-water analogy. The dimensionless source strength for fire, $Q^* = \frac{\beta_T \dot{Q}}{\rho_0 c_p g^{1/2} H^{5/2}}$, is analogous to the source strength for salt-water, $m_{sw}^* = \frac{\beta_{sw} \dot{m}_{salt}}{\rho_0 g^{1/2} H^{5/2}}$, and the parameters $\frac{\dot{Q}}{c_p T_o}$ and $\dot{m}_{salt}$ are dimensionally equivalent. Steckler [39] provides a detailed examination of the mathematical formulation.

With the analogy in place, salt-water experiments can be performed in a scale model, taking care to ensure that the salt-water is injected so as to form a turbulent and buoyancy-dominated plume, as these are the important features of smoke flow that is modeled by the salt-water flow. Although it is known that turbulent fire plumes have $Re \sim 10^5$, Steckler et al. contends that $Re \sim 10^4$ is acceptable. As the *Re* number becomes unimportant so long as it is large, the salt-water experiments can be run with different mass flow rates and salt concentrations if the salt-water model is designed to give a large *Re* number. Following turbulence as the first condition, the second major requirement is to make sure that the salt-water plume is buoyancy driven. Since the flow velocity will need to be high enough to ensure turbulence, the initial flow will be momentum driven. At some distance below the injection point, the flow will become buoyancy driven. The nozzle diameter also impacts the buoyancy and turbulence of the plume. A tiny nozzle will tend to give a turbulent jet, while a larger nozzle will tend to produce a buoyant, laminar plume. Therefore, there must be a balance between salt concentrations, flow rate and diameter to achieve the desired flow characteristics.

2.2 Dispersion in a Complex Configuration

The dispersion in a complex configuration depends on many variables. A few of them have been highlighted in Figure 2.1 below.

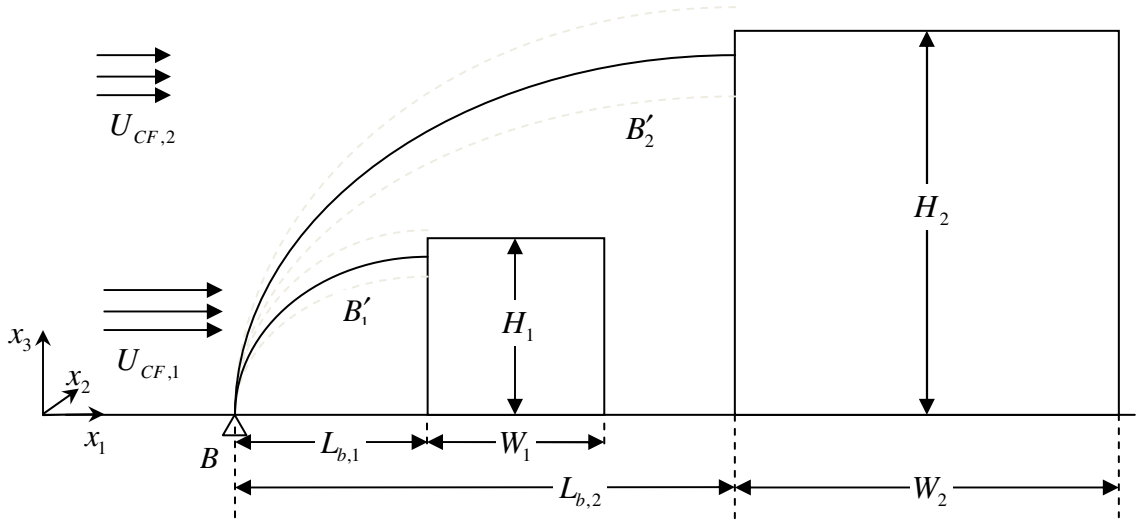

Figure 2.1: Dispersion of a buoyant plume in a crossflow near a building

As the plume in crossflow is a mixed convection problem, the appearance of *Froude* number, $Fr = \frac{U_{CF}}{U_{plume}}$, is expected. In order to define a *Fr* number, a length scale must be chosen as U_{plume} varies continuously with x_1 and (and associated x_3). Invoking a characteristic length scale, *L*, the *Fr* number can be easily defined in terms of the specific buoyancy flux, *B*:

$$Fr = \frac{U_{CF}}{\left[\frac{B}{L}\left(\frac{\rho_{sw}}{\rho_o}\right)\right]^{1/3}} \tag{2.1}$$

However B' provides a physically significant means of comparing the relative importance of the source strength with respect to the crossflow velocity without the requirement of a length scale. For this reason, B' is used in this study and appears in the scaling laws introduced in the following sections.

In the Figure 2.1, the source is assumed to be injected in the vertical direction, x_3, perpendicular to the crossflow direction, x_1. The important variables that govern the physics of a plume dispersion problem are the specific buoyancy flux, B, the modified buoyancy flux, B', the source distance normalized with the height of the building, L/H, the aspect ratio of the building, W/H, and the height of the building, H. In this problem, the height of the building may be used as a length scale to determine the dimensionless source strengths Q^* and m_{sw}^*. However, in the case of an unconfined plume and plume in crossflow where the length scale is not well defined in the problem, the source strength is represented by the specific buoyancy flux, B. Considering the plume is originating from a round steady source with uniform properties, the specific buoyancy flux, B, can be expressed as follows [27, 49]:

$$B = \dot{V}_o g \left(\frac{\rho_o - \rho_\infty}{\rho_\infty} \right) \tag{2.2}$$

where $\dot{V}_o$ is the source volumetric flow rate, g is the gravitational acceleration, ρ_o is the source density and ρ_∞ is the ambient density.

The specific buoyancy flux is the rate at which the buoyancy body force is introduced through the source, and it is a conserved property in the flow. It describes the magnitude of the dispersed quantity and is related to the volumetric flow rate and

density difference at the source. Increasing the specific buoyancy flux will result in an increase in the magnitude of the scalar, e.g. the concentration of the dispersed material, at any location along the plume centerline. Although the specific buoyancy flux alone may be adequate for defining the source strength for an unconfined plume, a modification to the buoyancy flux is necessary if the plume is in the presence of a crossflow in order to take into account the effect of the mass flux of the crossflow interacting with the buoyancy of the plume.

The steady state trajectory of the dispersed plume is determined by a modified buoyancy flux term, B', expressed as:

$$B' = \frac{\dot{V}_o g(\rho_o - \rho_\infty)}{\rho_\infty U_{CF}} \tag{2.3}$$

The modified buoyancy flux describes the relative importance of the body force with respect to the crossflow velocity. As the modified buoyancy flux takes into account the crossflow velocity, for the same specific buoyancy flux, B, different trajectories can be defined by B_1' and B_2' corresponding to different crossflow velocities as shown in Figure 2.1.

For a plume in crossflow, far away from the source where the flow is self-preserving, the vertical velocity becomes small and the trajectory of the plume becomes nearly horizontal. The vertical penetration distance and the radial penetration distance (about the centreline of the plume) are functions of the general displacement in the x_1-direction.

The trajectory of the plume in crossflow and turbulent motions in the dispersion of the plume is most commonly observed in the x_2-plane. However,

studies have shown that there is bifurcation of the plume into two counter-rotating vortices as the plume is dispersed from the source. This phenomenon can be observed in the x_3-plane. The details of these flow structures are known to be important, as the point where the vortices combine is regarded as an indication of the start of the self-similar regime in the far field. As such, although only images in the x_2-plane are taken in this study, it is noted that cross-plane images will be useful for a more complete analysis of the plume in crossflow.

2.3 Scaling Laws

Scaling Law for Unconfined Plume

The plume theory is established on the unconfined point-source plume configuration where the behavior of the fire plume is independent of source details and source geometry. Zukoski [50] provided a theoretical solution for the plume momentum and energy equations by using an integral method assuming Gaussian profiles for the velocity across the plume. The solution for the plume centerline velocity is

$$\frac{(\bar{u}_3)_c}{\sqrt{g x_3^+}} = C_V Q^{*1/3} \tag{2.4}$$

where

$$C_V = [25/(24\pi)]^{1/3} (\beta^{-1} + 1)^{1/3} \alpha^{-2/3}$$

The constant C_V is related to the entrainment constant, α, and the ratio of the velocity half-width to the temperature half-width, β. Zukoski [51] recommended $\alpha = 0.11$ and $\beta = 0.956$, resulting in $C_V = 3.87$ and equation 2.8 becomes:

$$\frac{(\overline{u}_3)_c}{\sqrt{g x_3^+}} = 3.87 Q^{*1/3} \tag{2.5}$$

Equation 2.9 is the scaling law for velocity which is used for the validation of the unconfined plume with theory.

Scaling Law for Plume In Crossflow

Diez et al. [49] found the scaling relationship for the vertical mean maximum penetration distance for a steady plume in crossflow as follows:

$$(x_3 - z_o) / x_s^* = C_{xs} \tag{2.6}$$

$$x_s^* = \left(B'^{1/2} x_1 / U_{CF} \right)^{2/3} \tag{2.7}$$

where x_s^* is a characteristic vertical distance that involves the conserved property B'. Diez et al. finds $z_o = 25.6D$ and C_{xs} to be 1.9 for steady plumes. The trajectory of the plume in crossflow can therefore be plotted using values of D, B' and U_{CF} for each experimental configuration. The measurement range of Diez et al. is up to $x_3^+ / D = 120$, and the researchers recommends that self-similar region are reached for $x_3^+ / D >$ 40-50 although the data from the measurements show that self-similar region may be reached as close as $x_3^+ / D > 20$.

The Briggs plume rise model is recommended by the U.S. Environmental Protection Agency, and appears to be acceptable for large thermally dominated plumes. Briggs equations predicted the plume rise as a function of a buoyancy flux term, F_B, wind speed and distance downwind, as it is thought that even after a plume is bent over by the wind, it continues to rise due to its thermal buoyancy. After a "long enough" time and distance downwind, the plume reaches its final rise. Different equations are used in the Briggs model depending on atmospheric stability. For neutral conditions, the downwind distance to the point of final plume rise is x_f, expressed as:

$$x_f = 119(F_B)^{2/5} \; for \; F_B \geq 55 \text{ m}^4/\text{s}^3 \tag{2.8}$$

or

$$x_f = 49(F_B)^{5/8} \; for \; F_B < 55 \text{ m}^4/\text{s}^3 \tag{2.9}$$

The plume rise is calculated by

$$\Delta h = \frac{1.6(F_B)^{1/3}}{U_{CF}}(x_f)^{2/3} \; for \; x \geq x_f \tag{2.10}$$

or

$$\Delta h = \frac{1.6(F_B)^{1/3}}{U_{CF}}(x)^{2/3} \; for \; x < x_f \tag{2.11}$$

The buoyancy flux term, F_B, is given by Briggs as

$$F_B = g\left(1 - \frac{MW_s}{28.9}\right)\left(\frac{T_a}{T_s}\right)\frac{v_s d_s^2}{4} + 8.9\left(\frac{P_0}{P_a}\right)Q_H \tag{2.12}$$

where F_B is the buoyancy flux (m^4/s^3), g is the gravitational acceleration, MW_s is the molecular weight of the stack gas, T_a is the atmospheric pressure (mb), T_s is the stack gas temperature (K), v_s is the stack gas velocity (m/s), d_s is the stack inner diameter (m), P_0 is the standard sea level pressure (mb), P_a is the atmospheric pressure (mb) and Q_H is the heat emission rate (MW).

For salt-water sources used in the experiment, the buoyancy flux from Table 2.1 corresponding to the conditions in each test case is used instead of employing equation 2.11 to obtain F_B, as equation 2.11 is deemed to be suitable for large thermal sources rather than weakly buoyant sources like the salt-water source. The trajectory of the plume in crossflow using Briggs model is plotted using equations 2.8 and 2.10.

Virtual Origin

Plumes generated by steady volumetric releases of momentum and/or buoyancy from sources of finite area, where the location of release is defined as $x_3 = 0$, into a quiescent uniform ambient, are shown to be equivalent to pure plumes issuing from a point source at the virtual origin ($x_3^+ = 0$) located below the actual source, where $x_3^+ = x_3 - z_0$. By using a virtual origin, the effects of the injector geometry and initial injection momentum may be disregarded. Heskestad [52] has introduced a method for calculating the virtual origin from experimental data. As the location of the virtual origin largely depends on the point of buoyancy dominance and the point of transition from laminar to turbulent flow, it is hardly exactly the same for each experiment. The methods used for calculating the virtual origin for the unconfined plume and the plume in crossflow are highlighted below.

Virtual Origin Calculation for Unconfined Plume

Starting with equation 2.5, substituting $Q^* = m_{sw}^* = \frac{\beta_{sw}\dot{m}_{salt}}{\rho_0 g^{1/2} x_3^{5/2}}$ and rearranging:

$$\frac{(\overline{u}_3)_c}{\sqrt{g x_3^+}} = C_V m_{sw}^{*\,1/3}$$

$$\frac{(\overline{u}_3)_c}{\sqrt{g x_3^+}} = C_V \left(\frac{\beta_{sw}\dot{m}_{salt}}{\rho_0 g^{1/2} x_3^{+5/2}} \right)^{1/3}$$

$$x_3^+ = C_V^3 \left(\frac{g\beta_{sw}\dot{m}_{salt}}{\rho_0} \right) (\overline{u}_3)_c^{-3}$$

$$x_3 - x_o = C_V^3 \left(\frac{g\beta_{sw}\dot{m}_{salt}}{\rho_0} \right) (\overline{u}_3)_c^{-3} \qquad (2.13)$$

By plotting $(\overline{u}_3)_c^{-3}$ against x_3, the virtual origin can be obtained from the intercept of the best fit line with the x_3 axis. Equation 2.13 can also be expressed as:

$$\frac{1}{C_V^3} x_3 - \frac{x_o}{C_V^3} = \left(\frac{g\beta_{sw}\dot{m}_{salt}}{\rho_0} \right) (\overline{u}_3)_c^{-3} \qquad (2.14)$$

By plotting $\left(\frac{g\beta_{sw}\dot{m}_{salt}}{\rho_0} \right) (\overline{u}_3)_c^{-3}$ against x_3, the gradient is equal to $\frac{1}{C_V^3}$ and the y-intercept is equal to $-\frac{x_o}{C_V^3}$.

Virtual Origin Calculation for Plume In Crossflow

Starting with equations 2.6 and 2.7,

$$(x_3 - z_o) / x_s^* = C_{xs}$$

$$(x_3 - z_o) = C_{xs} x_s^*$$

$$(x_3 - z_o) = C_{xs}\left(B'^{1/2} x_1 / U_{CF}\right)^{2/3} \tag{2.15}$$

By plotting $B'^{1/3}\left(\frac{x_1}{U_{CF}}\right)^{2/3}$ against x_3, the virtual origin is obtained from the intercept of the best fit line with the x_3 axis. The gradient of the line is equal to $\frac{1}{C_{xs}}$.

2.4 Experimental Facility

The experimental facility for this research is built upon the existing setup that has been used in previous salt-water modeling studies, with modifications and add-on systems that are necessary to create a cross flow in the test region. Central to the experimental facility is a large capacity tank (1.7 m × 0.9 m × 1.2 m) with walls made of one-inch thick acrylic and reinforced by iron supports to withstand the water pressure. The tank, when filled with fresh water, provides the test region for the salt-water plume experiments. The supporting systems of the facility include a salt-water source system, a blower system providing the crossflow, a laser and optics system to illuminate the salt-water plume in the test region, and a diagnostics system for image acquisition and post-processing.

2.4.1 Salt-Water Source System

The salt-water source system, comprising an upper container, a lower overflow container, a pump, a flow meter and an injector, provides the salt-water to be injected into the fresh water tank at a constant flow rate. The upper 10-gallon container is positioned at a height above the fresh water tank to maintain a constant

gravity head which pushes the salt-water through the flow meter into an injector placed in the test region. Salt-water is constantly pumped from the overflow container to the upper container. A return pipe in the upper container allows excess salt-water to flow back into the overflow container, thus maintaining a constant salt-water level in the upper container and isolating any fluctuations from the pump during the experiment. As the salt-water is injected into the fresh water tank, recirculation continues between the upper and overflow container until the latter is depleted, which then calls for a replenishment of salt-water into the overflow container.

A Gilmont glass flow meter (Model GF-6541-1230) is used to adjust and monitor the volumetric flow rate. The reading of the flow meter is on a (0-100) scale with a ± 5% uncertainty. As the flow meter calibration provided by the manufacturer applies to only pure water, the flow meter is recalibrated for salt-water solution of 13% concentration by mass. The flow meter calibration is shown in Figure 2.2 below.

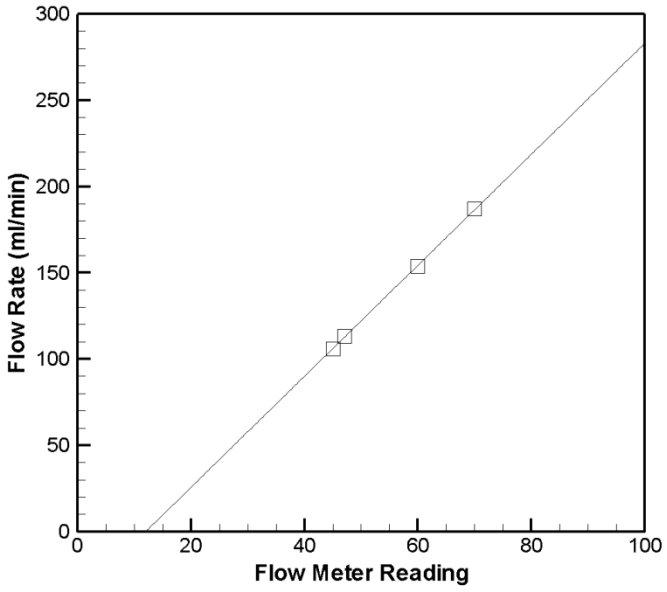

Figure 2.2: Flow meter calibration for salt-water at 13% mass concentration

The injector is a stainless steel tube with an internal diameter of 5.6 mm. During the experiments, it is partially submerged in the fresh water, held in place by 8020 aluminum supports built across the top of the water tank. As a possibility for future expansion, a manifold providing six outlets is installed in the salt-water source system. This allows the facility to be used to study multiple plumes dispersion.

2.4.2 Cross Flow Generation System

The study of wind-driven plume dispersion using the salt-water modeling technique requires a cross flow to be generated in the fresh water tank, simulating wind effects in the atmospheric environment. The cross flow generation system that is conceived for this research is based on an internal circulation method that pushes water one end of the tank to another, creating a cross flow in the tank. The system comprises a plenum, four sump pumps and an array of pipes and flexible tubes connecting the pumps and the plenum which are installed at opposite ends of the tank. The plenum, also known as the “blower”, is a ¼-inch thick aluminum box with a depth of 0.2 m and one open face measuring 0.5 m by 0.5 m. The open face of the blower is flanged, allowing perforated metal plates to be secured at the opening. Water is drawn by the sump pumps and fed through 1¼-inch pipes into four inlets on each side of the blower. Within the void of the blower, the momentum of the incoming jets is dissipated by applying back pressure using obstructing materials in order to achieve a uniform flow at the open face of the blower.

2.4.3 Model of Building

The model of a building with dimensions 10 cm (L) by 20 cm (W) by 20 cm (H) is constructed using 1/4-inch clear acrylic. The floor is built with a sheet of 3/8-inch acrylic measuring 95 cm by 61 cm. The building model is inserted into a rectangular hole cut in the acrylic sheet, so that the height of the building is adjustable from 2 cm to 20 cm. Both the floor and the building are mounted on 8020 aluminium supports. A 6-mm hole is drilled at a position of 10 cm from the edge of the building for the source injector location.

Typical height to width aspect ratios for buildings ranges from 0.2 to 1 for normal buildings such as 4-storey classroom building. For a 55-storey high-rise building, the aspect ratio may be as high as 7. The model used in this experiment has an aspect ratio of 0.5.

2.5 Diagnostic Tools

2.5.1 Blue Dye Flow Visualization Technique

As the salt-water is colorless, there is a need to mix in a dye in order for the flow of the salt-water to be clearly seen. In this experiment, a blue dye is used. The salt solution is first prepared to the desired level of salinity, after which the blue dye is added to the solution. The salt solution is then ready for injection. A row of six fluorescent tube lamps are installed behind the back surface of the tank to provide back lighting. Translucent plastic sheets are placed between the fluorescent lamps and the tank to diffuse the light so that the back lighting is uniform. In this way, the images captured by the camera will show a good contrast between the blue salt plume

and the white background. The PIV system is then configured to capture single frames using the CCD camera. A series of background images with the back lighting is first captured for 2 minutes, and the images are processed to produce an average background image which can be used subsequently for subtraction from the plume mean image. The blue salt solution is then injected and the images of the plume are captured for 5 minutes. The raw images of the plume can then be processed to obtain the mean plume image with or without the background.

It is important that the blue dye does not affect the salinity of the salt solution or the source injection flow rate. Otherwise, the amount of blue dye mixed into each batch of salt solution will have to be strictly controlled. Kelly [40] has shown that the blue dye has no effect on the salinity using a conductivity probe to measure the salinity of the salt solution with and without the blue dye on separate occasions. The flow meter calibration of the salt solution also shows that the blue dye does not change the flow rate of the source injection.

2.5.2 Particle Image Velocimetry (PIV) System

Particle Image Velocimetry is an optical method that has been in use for more than two decades to measure velocities in a fluid seeded with small particles. The method works by simultaneously illuminating the seeding particles with a laser light sheet and taking a pair of images shortly after each other. With the known time between each pair of images and the measured displacement of the particles, the velocities of the particles can be calculated, thus enabling the entire velocity flow field in the fluid to be mapped out. A double-pulsed green Nd/YAG laser with a

wavelength of λ = 532 nm is used. A cylindrical lens is used to focus the laser into a light sheet. A CCD camera with a resolution of 2048 x 2048 (4 megapixels) and a Canon 60 mm lens with f/2.8 are used to capture the images. It is recommended for the seeding particles to be chosen such that the image of each particle on the CCD chip of the camera is greater than one pixel. The diameter of a particle's image on a CCD chip, d_i, the magnification of the optical system, M, and the diffraction limited image diameter, d_{diff}, are respectively given by

$$d_i = \sqrt{(Md_p)^2 + d_{diff}^{\ 2}} \tag{2.5}$$

$$M = \frac{Chip\ Size}{Field\ of\ View} \tag{2.6}$$

$$d_{diff} = 2.44 f_{\#}(M+1)\lambda \tag{2.7}$$

where d_p is the physical diameter of the particle, $f_{\#}$ is the f number of the lens system, and λ is the wavelength of the incident light on the particle. The chip size is 1.52 cm and f/2.8 lens is used. The seeding particle used is polyamide particles with a diameter of 50 μm. For the particle image diameter to be about 1 pixel, the calculated field of view is 12 cm. During the experiment, a field of view of 20 cm, corresponding to a particle image diameter of 0.74 pixel, was still able to produce good results.

2.6 Experimental Methodology

The current salt-water modeling facility has been utilized in many past research studies for quantitative measurements of the flow dynamics in classical fire configurations in a still environment using laser diagnostics such as PLIF and LDV. This study is the pioneering work for analyzing plumes in a crossflow with the PIV technique using the existing salt-water modeling facility. As such, the extent to which this study will be successful hinges on two key activities: the validation of the PIV laser diagnostic technique and the development of a crossflow generator for the salt-water facility. The experimental methodology starting from the PIV technique validation to the final investigation of crosswind dispersion near a building is discussed in this section.

In a previous study by Yao [43, 44, 45], excellent agreement has been obtained between salt-water measurements and real fire data for unconfined buoyant plumes. Yao had carefully chosen initial conditions for his experiments to ensure that the salt-water plume is buoyancy dominated and turbulent, which is essential for the mixing dynamics to be similar to that in a real fire-induced flow. The validation of the PIV technique, being the first part of this study, is therefore based on two cases of Yao's experiments that involved unconfined buoyant plumes. Using similar initial conditions, good agreement with Yao's experimental data may be expected if the PIV technique is implemented correctly. In addition, the PIV measurements will also be compared with the correlations recommended by Zukoski [51] based on the turbulent point source plume theory.

The design and construction of the crossflow generator, or “blower”, requires considerable time and is carried out concurrently with the PIV technique validation. Once the prototype is constructed, a detailed characterization of the blower performance is necessary to obtain a region of uniform crossflow as the test section. Several iterations on the blower configuration is required to improve the crossflow uniformity, and two configurations providing different crossflow velocities are selected for performing the next part of the experiment, i.e. analyzing a buoyant plume in a crossflow.

The plume in crossflow is investigated using both the flow visualization and PIV techniques for qualitative analysis of the plume trajectory and quantitative analysis of the plume centerline velocities respectively. Two experiments are carried out at different crossflow velocities using two blower configurations. The source initial conditions used are similar to the first experiment of the unconfined plume. The trajectories obtained from the flow visualization are compared with the scaling law described by Diez et al [49] and with the classical Brigg’s plume rise formula. The variations of the velocity components along the trajectory are also analyzed.

Finally, a simple model of a building is used to study the behavior of a plume in crossflow near a building. From the flow visualization images, the trajectory of the plume near a building is compared with that of similar plume under the same conditions without a building. With the PIV measurements, the flow structures near the building are identified and analyzed. Overall, a total of 4 blower characterization and 6 salt-water modeling experiments are carried out. Details regarding the

conditions of the 6 salt-water modeling experiments are summarized in the table below.

Table 2.1 Initial experimental conditions in salt water modeling measurements

	Case 1	**Case 2**	**Case 3**	**Case 4**	**Case 5**	**Case 6**
Experimental Configurations and Measurements						
Flow Configuration	Unconfined Plume	Unconfined Plume	Plume In Crossflow	Plume In Crossflow	Plume In Crossflow Near Building	Plume In Crossflow Near Building
Injector Diameter, D (mm)	5.6	5.6	5.6	5.6	5.6	5.6
Measurements	PIV	PIV	PIV and Flow Vis.	Flow Vis.	PIV and Flow Vis.	Flow Vis.
Initial Flow Conditions of Salt-Water Plume						
Volumetric Flow Rate, $\dot{V}$ (ml/min)	110	165	110	110	110	110
Salt Mass Fraction, Y_{salt}	0.13	0.13	0.13	0.13	0.13	0.13
Injection Velocity, U_{inj} (mm/s)	74	112	74	74	74	74
Characteristic Scales						
Specific Buoyancy Flux, B ($\times 10^{-6}$ m^4/s^3)	1.78	1.78	1.78	1.78	1.78	1.78
Modified Buoyancy Flux, B' ($\times 10^{-5}$ m^3/s^2)	N/A	N/A	5.10	4.25	5.10	4.25
Crossflow Velocity, U_{CF} (mm/s)	N/A	N/A	35	42	35	42
Characteristic Length Scale, D^* (mm)	1.33	1.55	1.33	1.33	N/A	N/A
Building Height, H (m)	N/A	N/A	N/A	N/A	0.1	0.1
Source Distance, L/H	N/A	N/A	N/A	N/A	1	1

Chapter 3: Results and Analysis

The nature of the salt-water modeling experiments is such that the flow is downwardly injected and the plume is negatively buoyant. An actual image of the flow will therefore show a falling buoyant plume. The figures in this section are presented in an inverted manner to show rising plumes due to the greater familiarity of most individuals with rising plumes which are positively buoyant. Rising or falling buoyant flows have similar buoyant flow properties as both involve progressive approach to the ambient density with increasing distance from the source.

3.1 Validation of PIV Technique with Unconfined Plume

The unconfined buoyant plume experiments are carried out under Case 1 and Case 2 conditions highlighted in Table 2.1. Figure 3.1(a) shows an instantaneous image captured by the CCD camera with a field of view of about 200 mm. The plume is observed to thin out slightly from the point of injection to the turbulence transition point at a distance of about 5−6D from the source. The turbulent flow and entrainment can also be clearly seen as the plume increases in radius after the transition point. Figure 3.1(b) shows the instantaneous velocity vectors calculated by the PIV software from a pair of images taken at an interval of 1.8 ms. The mean velocity field calculated by taking the statistical mean of 1000 pairs of images taken at a rate of 3 Hz is shown in Figure 3.1(c). The plume centerline velocity is observed to increase to a maximum after injection and subsequently decay with increasing distance from the source. For a more detailed analysis, the centerline velocity profile is extracted from mean velocity field and plotted in Figure 3.2.

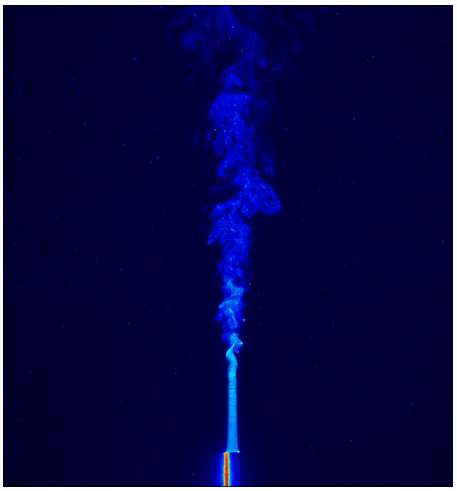

(a)

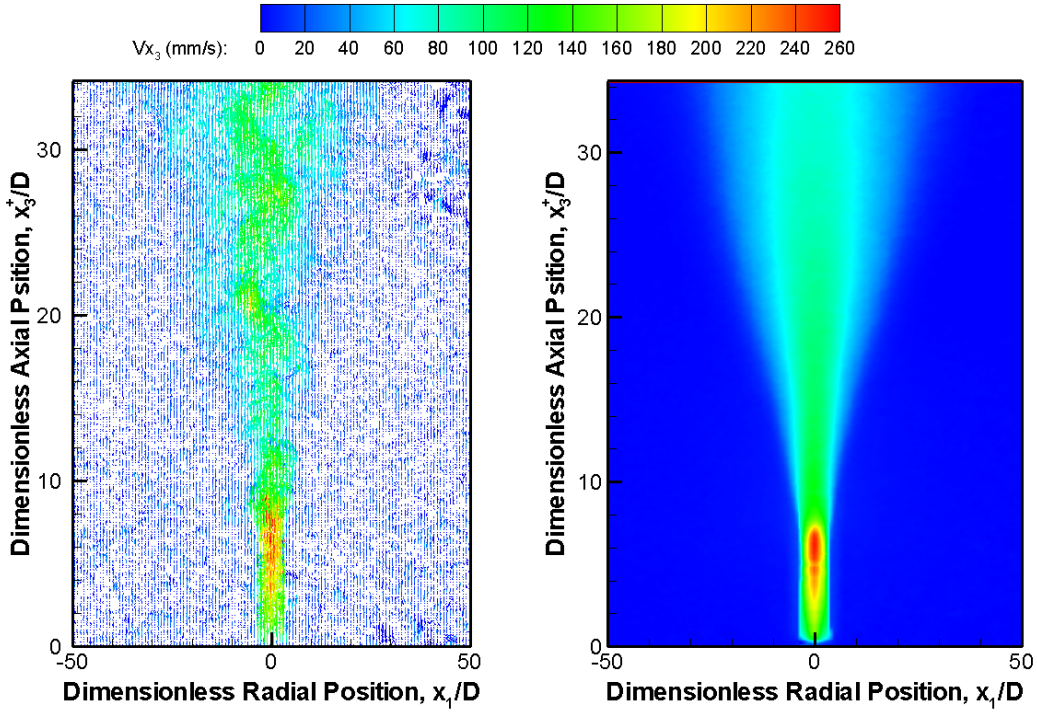

(b) (c)

Figure 3.1: PIV Images of unconfined buoyant plume; (a) Instantaneous raw CCD image; (b) Instantaneous velocity vectors; (c) Mean velocity field

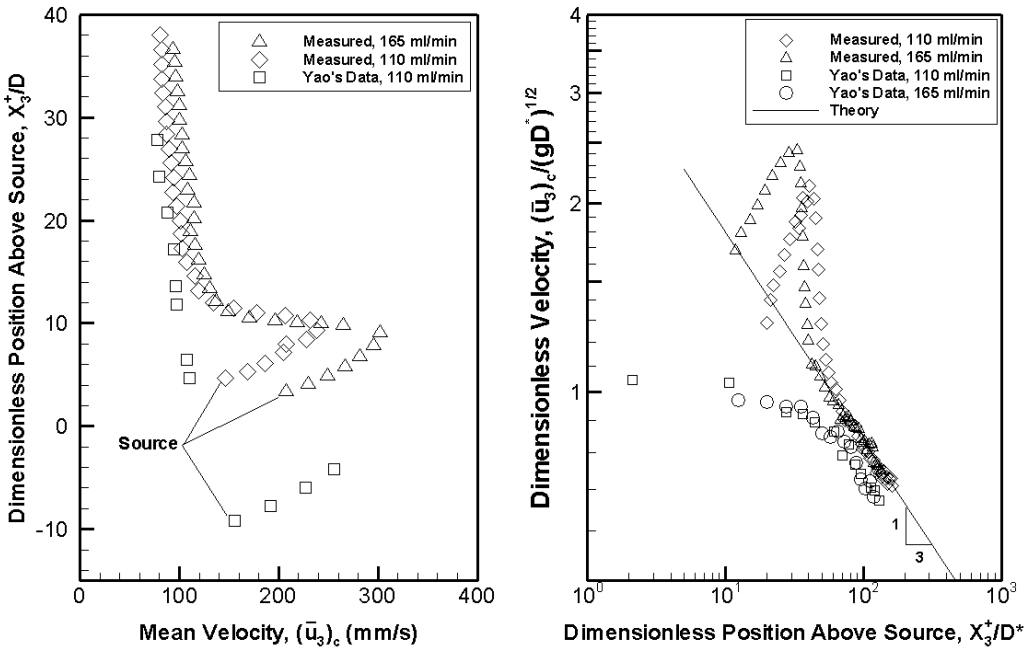

(a) (b)

Figure 3.2: Velocity distribution along plume centerline; (a) Mean velocity (b) Dimensionless velocity

The velocity distributions along the plume centerline are compared with both Yao's data and the turbulent point source theory. The velocities are plotted taking into account the locations of the virtual origin. In Figure 3.2(a), the far-field data points for both the experiment measurements and Yao's data appear to follow a similar decay. In the near-field, the data points from the experiment measurement for $\dot{V}$ =110 ml/min lies above Yao's data. This can be explained by the changes in the virtual origin position for each different experiment. The large differences in virtual origins between Yao's configuration and the current configuration are somewhat surprising. Yao measured a positive virtual origin but in these experiments, negative virtual origins are consistently obtained. Although the virtual origin may be different, the

magnitude of the measured exit and maximum mean velocity appears to agree with Yao's data. In Figure 3.2(b), the measured velocity decays for both cases follow the (1/3) power law described by the turbulent point source theory. The velocity coefficients for both cases in the current study are calculated to be 3.83 and 3.86 respectively, agreeing well with theory. Overall, as the PIV velocity measurements agree well with Yao's data as well as the point source plume theory, the PIV technique with salt-water modeling is validated. The table below summarizes the measured virtual origins and velocity coefficients in comparison with Yao's data and the point source theory.

Table 3.1 Results of PIV measurements for the unconfined buoyant plume

	Case 1 Measured	Case 2 Measured	Case 1 Yao's Data	Theory
Virtual Origin (mm)	-22.5	-14.7	53.6	-
C_v	3.83	3.86	3.4	3.87
Power	1/3	1/3	1/3	1/3

3.2 Characterization of Blower

The initial prototype of the blower comprised an aluminum box with a sheet of perforated metal and 3 sheets of wire mesh held to the blower using a flange. Iterations to the blower configuration are then made in an attempt to achieve a uniform velocity profile at the exit of the blower by diffusing the momentum of the 4 incoming jets from the pumps. In each iteration, the blower is disconnected from the pipes and removed from the tank before any physical modifications can be made. After the modification, the blower is re-installed and aligned in the tank. The mean velocity field of the crossflow generated by the blower is then taken using the PIV

technique for analysis. Due to the large flow region of the blower, the images have to be taken separately at the top and bottom sections of the blower. The statistical mean of the images are then combined during the processing phase to obtain the entire mean velocity field of the blower. A total of 4 configurations are tested and characterized as shown in Figures 3.3 and 3.4.

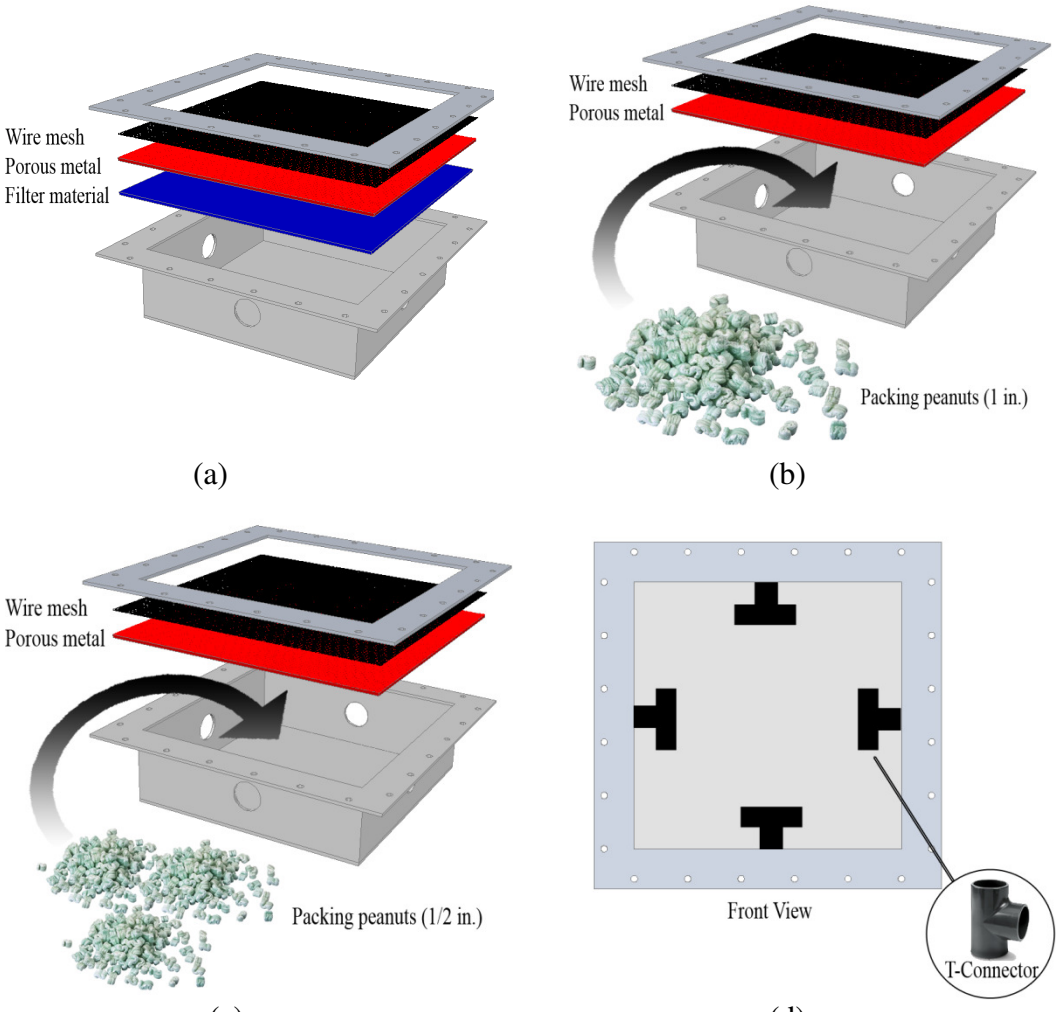

Figure 3.3: Blower configurations; (a) Configuration 1 with filter material; (b) Configuration 2 with 1-inch packing peanuts; (c) Configuration 3 with ½-inch packing peanuts; (d) Configuration 4 with ½-inch packing peanuts and four T-connectors

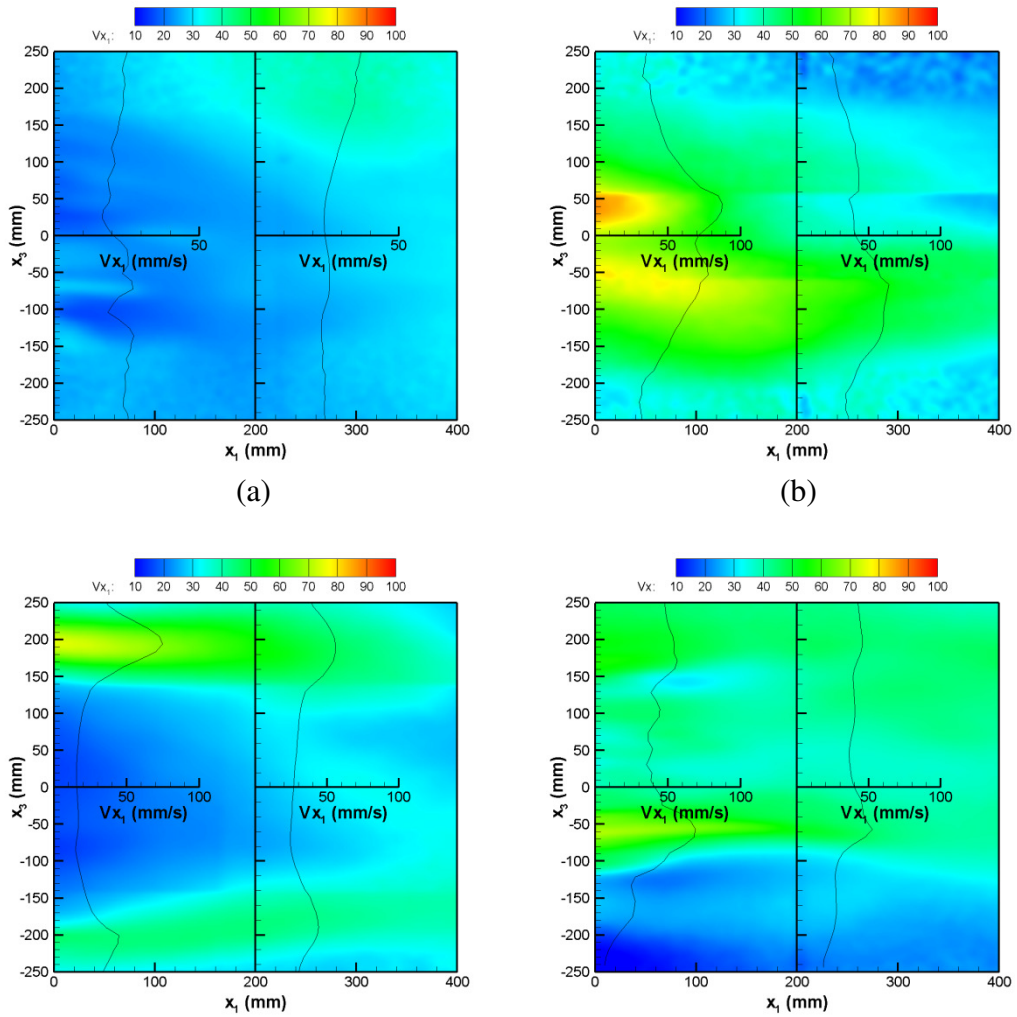

Figure 3.4: Velocity profiles of blower; (a) Configuration 1 profile; (b) Configuration 2 profile; (c) Configuration 3 profile; (d) Configuration 4 profile

Configuration 1

Configuration 1 shown in Figure 3.3(a) uses layers of filter material pressed together into a thickness of about 5 mm to diffuse the flow. The pore size of the filter material is estimated to be less than 50 microns. During the characterization of this configuration, it is found that the longer the blower is used, the less dense is the seeding in the tank, resulting in difficulties in obtaining sufficient vectors in the PIV

measurements. It is later discovered that the filter material is actually trapping the seeding particles and preventing them from flowing out of the blower. This is undesirable as a good seeding density in the flow is necessary for proper PIV measurements. Although the velocity profile shown in Figure 3.4(a) for Configuration 1 is reasonably uniform at 200 mm from the blower exit, this configuration is not feasible as it hindered the use of the PIV technique.

Configuration 2

Instead of using a filter material, in the second configuration shown in Figure 3.3(b), the internal void of the blower is filled with standard packing peanuts of about 1 inch long. Theoretically, the peanuts should reduce the momentum of the jets by forcing the water to swirl around within the blower before exiting. Figure 3.4(b) shows the velocity field for Configuration 2. The velocity field shows a strong flow coming out from the center of the blower, likely to be caused by the combination of the top and bottom incoming jets at the center of the blower. At the blower exit, the velocity at the center is almost twice that at the top and bottom. The velocity profile is not uniform, implying that the peanuts are not diffusing the flow enough.

Configuration 3

The packing peanuts used in Configuration 2 are ineffective due to their large size. In Configuration 3, shown in Figure 3.3(c), the peanuts are reduced in size to about 0.5 cm by 0.5 cm by 0.5 cm by manually breaking up each peanut into 4 pieces. With a reduction in the peanut size, the average pore size is reduced, forcing the water

to lose more momentum as it passes through the mass of peanuts before exiting the blower. From the velocity profile in Figure 3.4(c), a section of rather uniform crossflow is observed in the center of the blower. The influence of the incoming jets is concentrated at the top and bottom of the blower. Configuration 3 is usable when the injector is placed at 100 mm below the top of the blower and 200 mm from the exit of the blower. Figure 3.5(a) shows the location of the identified test section.

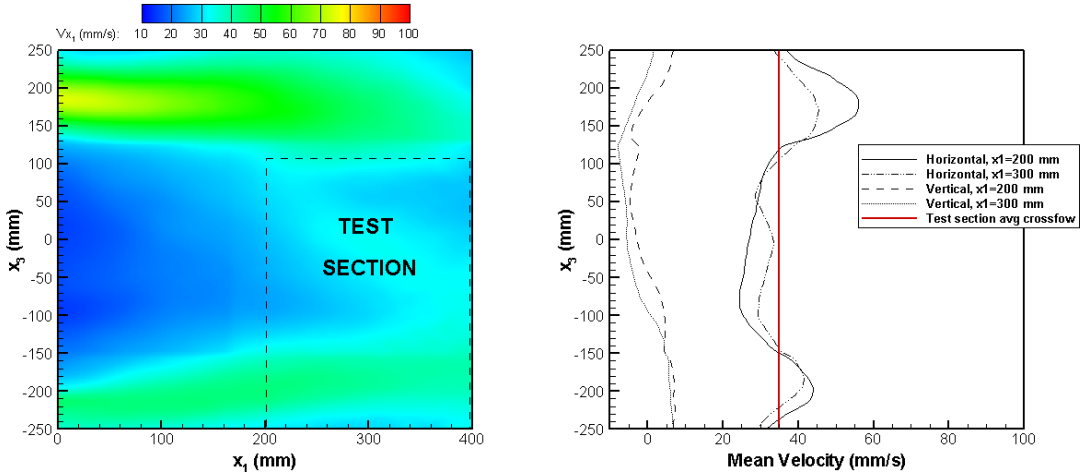

(a) (b)

Figure 3.5: Blower configuration 3 test section; (a) Test section location; (b) Horizontal, vertical and average velocity profiles

In order to determine an average crossflow velocity that is representative of the test section, an average of the crossflow profiles at 200 mm and 300 mm from the exit of the blower and over the height of the test section is taken. The calculated average crossflow velocity is 35 mm/s. Figure 3.5(b) also shows the vertical variations of the velocity profiles at the 200 mm and 300 mm from the exit of the blower. The vertical velocities vary from about -8 mm/s to 6 mm/s which is about 17–22% of the average crossflow velocity. When compared with the unconfined buoyant plume near-field velocities of 140–240 mm/s and far-field velocities of about

90 mm/s, the vertical variation is about 3–6 % and 7–9 % respectively, which is not significant.

Configuration 4

Further improvement is made on Configuration 3 by placing PVC T-connectors at each of the inlets of the blower to split the incoming jets into two directions as shown in Figure 3.3(d). The velocity profile in Figure 3.4(d) shows a reasonably uniform profile within about 350 mm from the top of the blower at a distance of 200 mm from the blower exit. For this configuration, the injector may be placed at the top of the blower at 200 mm from the blower exit. Figure 3.6(a) shows the selected test section.

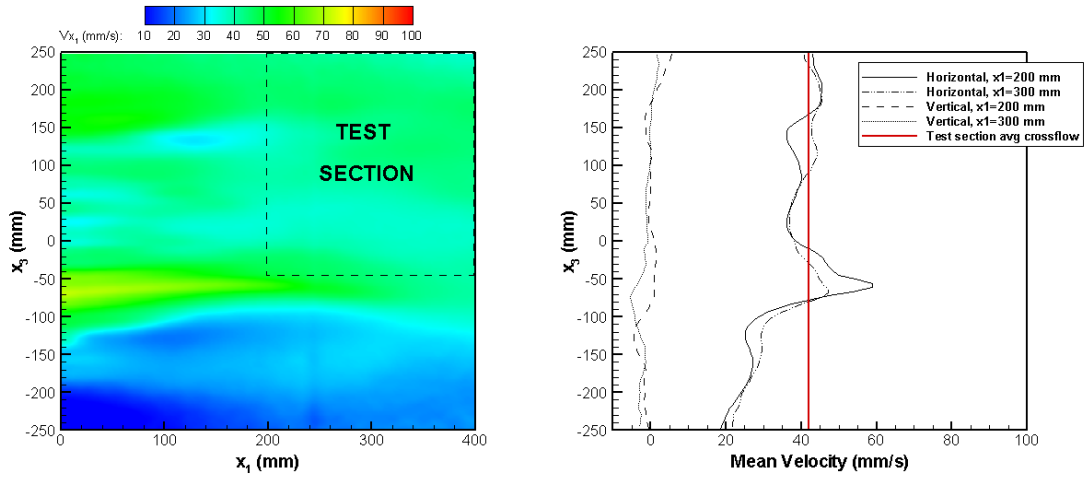

(a) (b)

Figure 3.6: Blower configuration 4 test section; (a) Test section location; (b) Horizontal, vertical and average velocity profiles

Similar to Configuration 3, the mean velocity of the test section is calculated by averaging the profiles at 200 mm and 300 mm from the exit over the height of the test section. A mean velocity of 42 mm/s is obtained. An examination of the vertical

velocities in Figure 3.6(b) shows that there is minimal vertical variation in the test section except for the top of the section at 200 mm from the exit where the vertical velocity is about 5 mm/s. As this variation is about 12% of the average crossflow velocity and 6% of the far-field velocities found in the unconfined buoyant plume, it can be considered small in comparison.

Configurations 3 and 4 are able to produce test sections with acceptable velocity profiles at mean velocities of 35 mm/s and 42 mm/s respectively. These two configurations are therefore used in the subsequent experiments involving plume dispersion in a crossflow. The performance of the blower can, of course, be further improved subject to more iterations and modifications which will be discussed in the last chapter.

3.3 Plume In Crossflow

The plume in crossflow is investigated using the blue-dye flow visualization and the PIV technique under the conditions of Cases 3 and 4 highlighted in Table 2.1. The initial conditions for both cases are similar except for the crossflow velocity which is 35 mm/s for Case 3 and 42 mm/s for Case 4. The trajectory analysis for Cases 3 and 4 is first discussed followed by the velocity field for Case 3.

Trajectory Analysis

Figure 3.7 shows the images taken using the blue dye flow visualization method. From the instantaneous image in Figure 3.7(a), it is observed that the turbulent motions of the lower surface of the plume are less pronounced than that at the upper surface, showing that the upper region of the plume is relatively more unstable to buoyancy disturbances. In addition, the flow from the source is observed to become turbulent at a distance of about 2−3D from the source. Compared to the unconfined plume in still environment, the turbulent transition point for the salt-water plume in crossflow is about half. The mean images in Figure 3.7(b) and 3.7(c) show the trajectory of the plume. As the trajectory is defined by the points of highest intensity in the plume, it can be extracted using either MATLAB or a plot digitizer. With MATLAB, a simple code is written to scan the columns of pixels from left to right, picking out the point of highest intensity count in each column of pixels. These points, when plotted together, form the trajectory of the plume. Using a plot digitizer, the trajectory may also be mapped out by manually selecting the points of highest

intensity from the image. The trajectories for Cases 3 and 4 are compared with the scaling law provided by Diez et al. and Brigg's plume rise equation in Figure 3.8.

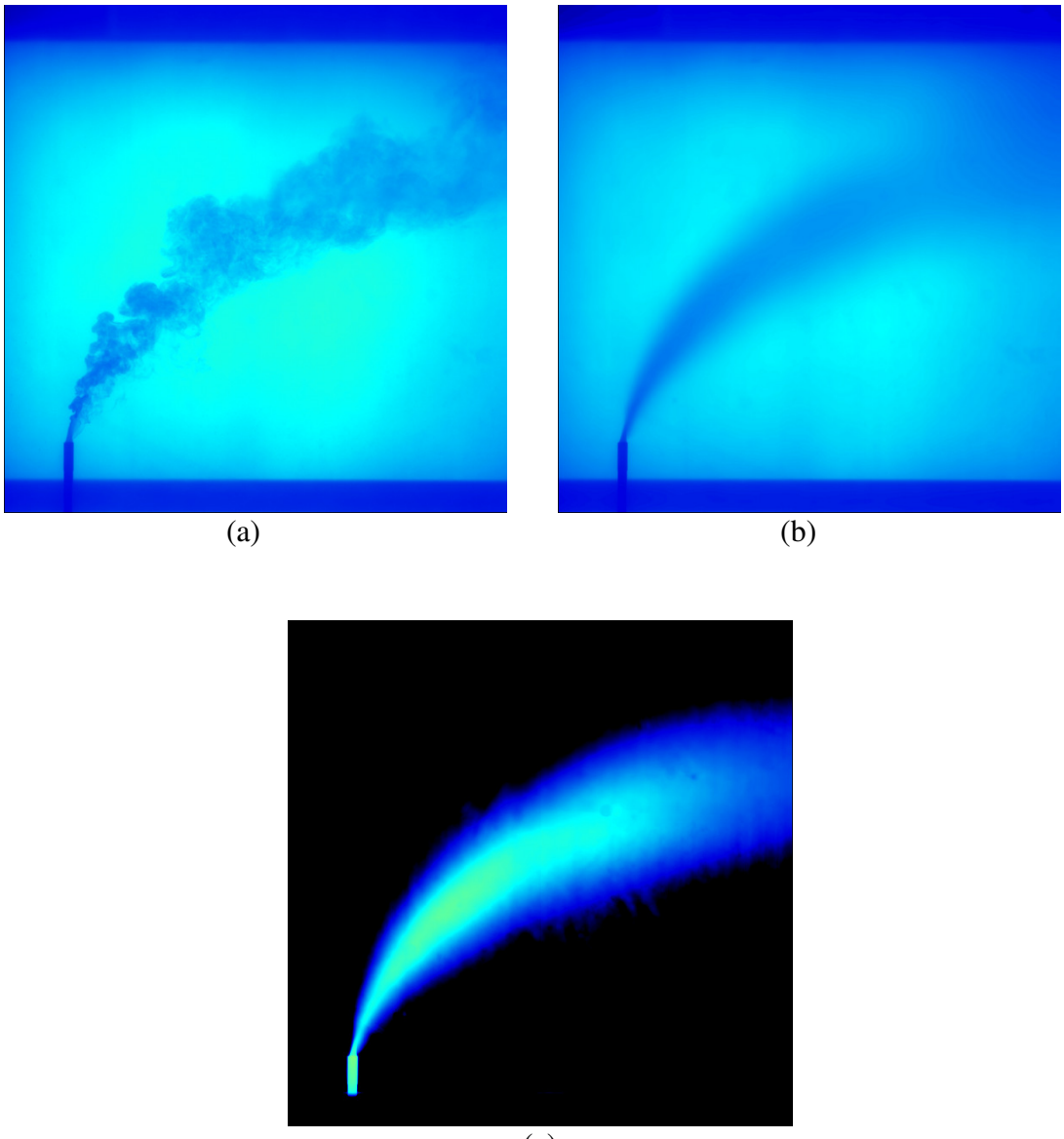

(a) (b)

(c)

Figure 3.7: Flow visualization of plume in crossflow for Case 3; (a) Instantaneous image; (b) Mean of all images; (c) Mean image with background removed

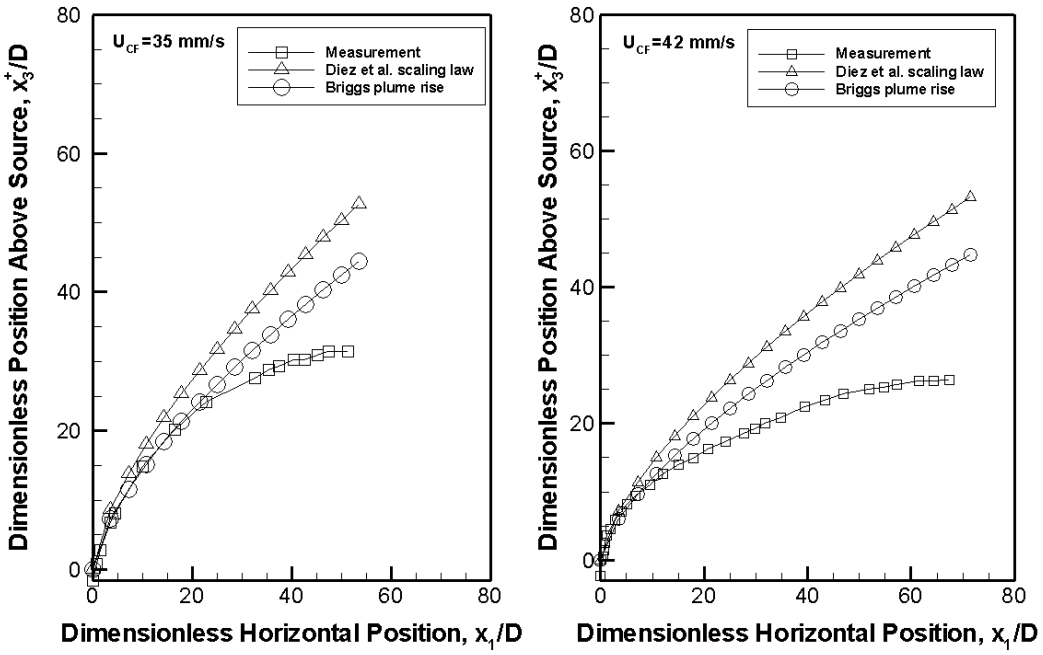

(a) (b)

Figure 3.8: Trajectory comparison for plume in crossflow; (a) Case 3, Crossflow velocity = 35 mm/s; (b) Case 4, Crossflow velocity = 42 mm/s

For both cases, the measured trajectories showed some agreement in the near-field and a similar trend of generally having a smaller vertical displacement in the far-field when compared with the scaling law or Briggs' plume rise. In the near-field, the measured trajectories agree closely with the scaling law and Briggs' plume rise up to a horizontal displacement of 10D and 20D respectively. The difference in the trajectories after a horizontal displacement of 20D may either be caused by the measured plumes losing their buoyancy faster than they should, or by the increasing non-uniformity in the crossflow velocity as the plume gets further away from the blower. The calculated vertical penetration coefficient for Cases 3 and 4 are 1.5 and

1.4 respectively, and the virtual origins are 6 mm and 13 mm respectively. Diez et al. found a vertical penetration coefficient of 1.9, and a virtual origin of 143±25.2 mm.

Velocity Analysis

The PIV measurements taken for Case 3 are shown in Figures 3.9 and 3.10. Figure 3.9(a) shows an instantaneous velocity field and Figure 3.9(b) shows the mean velocity field with the plume trajectory measured using the flow visualization method mapped onto the velocity field. The trajectory as seen from the velocity field agrees well with that obtained by flow visualization, though after a horizontal distance of 10D, the trajectory of the plume is not very obvious from the velocity field as the velocities in the plume and in the ambient crossflow are very similar. For further analysis, the vertical and horizontal velocity components along the plume trajectory are extracted and plotted in Figure 3.10.

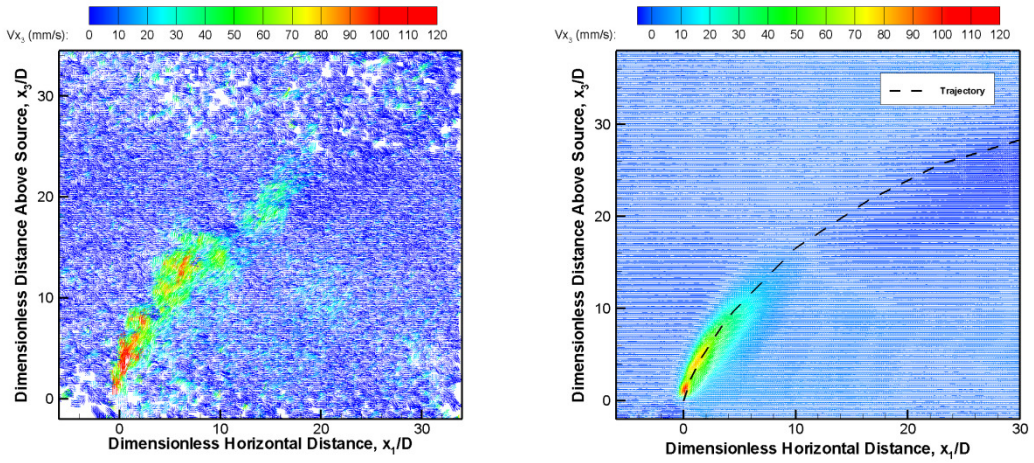

Figure 3.9: PIV images for plume in crossflow; (a) Instantaneous velocity field; (b) Mean velocity field

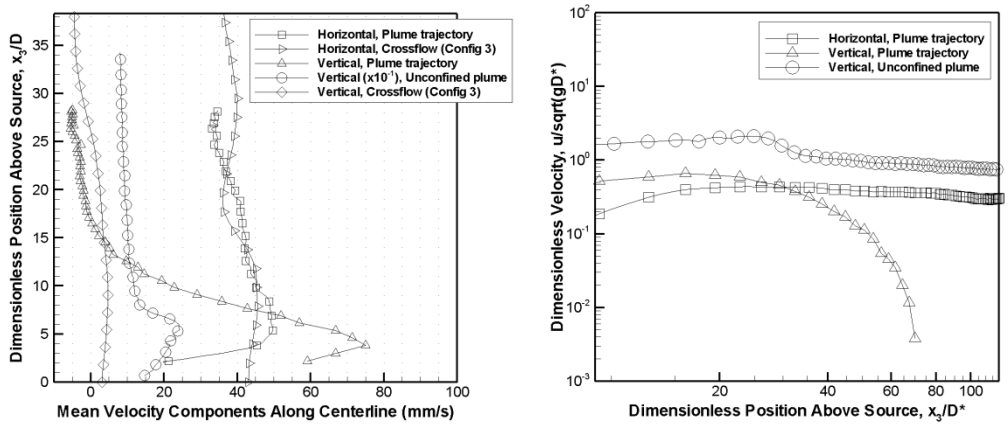

(a) (b)

Figure 3.10: Velocity variation along plume trajectory; (a) Comparison with unconfined plume and effects of variations in crossflow; (b) Dimensionless velocity comparison with unconfined plume

In Figure 3.10(a), it is observed that the plume trajectory vertical velocity increases to a maximum after injection, and then decreases to 0 at about 17D from the source. The vertical velocity after injection is about 60 mm/s, and increases to a maximum of 75 mm/s. These vertical velocities are an order of magnitude smaller than that of the unconfined plume in still environment, which had a velocity of 150 mm/s after injection and a maximum velocity of 240 mm/s. This comparison shows that the presence of crossflow significantly reduces the vertical velocity of the plume. Similar observations are made in Figure 3.10(b) where the non-dimensional velocities are plotted. The dimensionless vertical velocity component decayed quickly after injection from the source, and did not follow the (1/3) power law for unconfined plumes. Another interesting observation is that after decreasing to 0 at about 17D from the source, the vertical velocity becomes negative. Physically, this means that the plume is starting to fall after rising to a maximum and losing its buoyancy, which

should not happen unless the density of the plume suddenly increases to higher than the ambient. However, from the flow visualization images, the trajectory is not observed to fall. This suggests that the trajectories obtained from flow visualization and from the velocity field do not match up exactly. Another possible reason for this observation in the fall of the plume trajectory is the effect of the vertical variation in the crossflow, which is plotted in the figure. There is a positive vertical velocity in the crossflow at the inject exit, which subsequently drops to 0 and negative after 25D source. The vertical velocity of the plume after 17D from the source also appears to closely follow the vertical velocity of the crossflow. This suggests that the vertical component of the crossflow is actually pushing the plume downwards after it has reached its maximum rise.

The horizontal velocity component along the centerline increases to about 50 mm/s after injection and then decreases to 35 mm/s at 25D from the source. Theoretically, the horizontal velocity of the plume should not exceed the crossflow velocity of 35 mm/s, unless the plume has a velocity in the horizontal direction initially. As the injector was placed vertical, it is more likely that the variation in the horizontal velocity component is due to the non-uniformity in the crossflow. The horizontal crossflow velocity profile plotted in the figure shows a rise in the horizontal crossflow velocity, followed by a slight decrease. This variation in the crossflow appears to be the likely cause for the rise and fall of the horizontal velocities in the plume. In Figure 3.10(b), the dimensionless horizontal velocity in the plume showed a similar slight increase followed by a slight decrease.

3.4 Plume In Crossflow Near Building

In the last part of the experiments, a building is added to the scenario in the form of a plastic model with height to width aspect ratio of 1. The experiments for the plume in crossflow near a building are carried out under the same initial conditions as that for the plume in crossflow for proper comparison subsequently. Cases 5 and 6 are analyzed with flow visualization and Case 5 is further analyzed with PIV. Figures 3.11 and 3.12 show the flow visualization images for Cases 5 and 6.

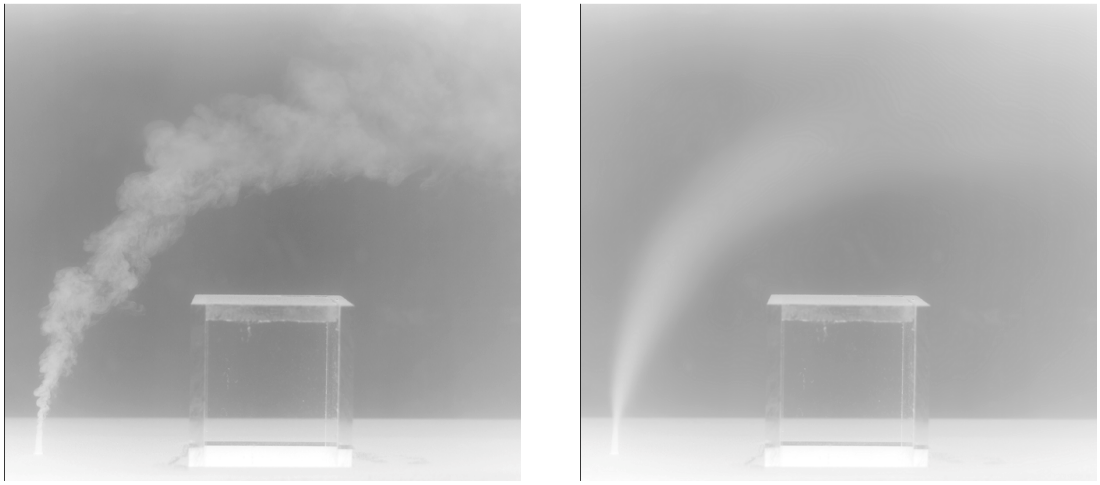

(a) (b)

Figure 3.11: Flow visualization for plume in crossflow near building for Case 5; (a) Instantaneous image; (b) Mean image

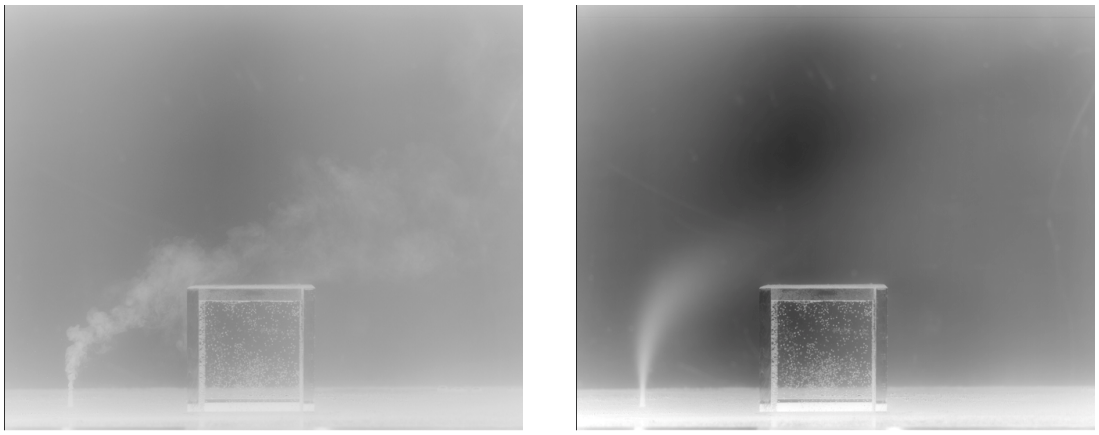

(a) (b)

Figure 3.12: Flow visualization for plume in crossflow near building for Case 6; (a) Instantaneous image; (b) Mean image

For Case 5, where the crossflow velocity is 35 mm/s, the plume trajectory does not interact with the building as shown in Figure 3.11(b). However, when the crossflow velocity if higher at 42 mm/s for Case 6, the mean image in Figure 3.12(b) shows that the plume interacts with the top edge of the building facing the source. In the instantaneous image in Figure 3.12(a), the plume shows some downwash on the side of the building facing the source. Such a downwash phenomenon occurred occasionally during the experiment for Case 6. The plume will always attempt to flow over the building due to its buoyancy. Even in the downwash region, instead of flowing down to the floor, the plume tries to continue to force its way up on the building face or around the sides of the building. Comparing the trajectory with and without the building for Case 5 conditions in Figure 3.13, it is clear that the presence of the building in the crossflow has pushed the plume trajectory higher and nearer the source.

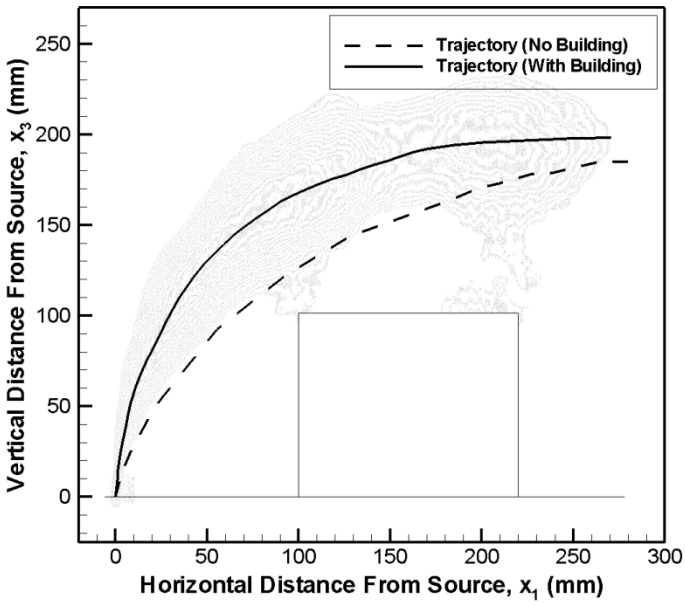

Figure 3.13: Plume trajectory comparison with and without building

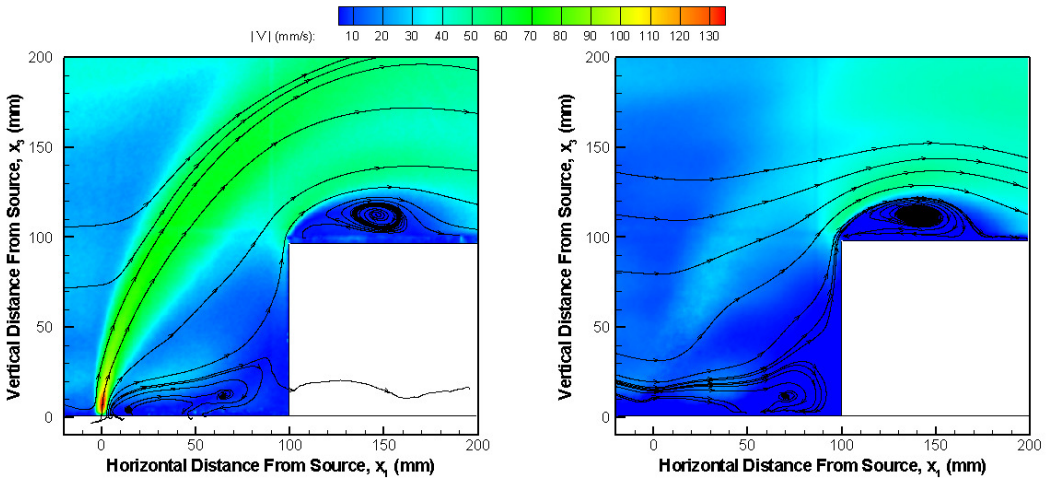

Figure 3.14: Flow structures around building; (a) Mean velocity field of PIV images taken at an interval of 1.8 ms; (b) Mean velocity field of PIV images taken at an interval of 12 ms

The mean velocity fields obtained from the PIV measurements shown in Figure 3.14 give some insight to the flow structures near the building. Figure 3.14(a) shows the mean velocity field from pairs of images taken at a smaller time interval of 1.8 ms compared with 12 ms in Figure 3.14(b). The vortices at the base and top of the building are observed after calculating the streamlines at different locations in the flow. As the velocities in these vortices are very small compared to the velocities in the plume, taking the images using a larger time interval will ensure that the smaller velocities are calculated with higher precision by the PIV software. However, this adjustment also means that the *plume velocity* measurements are more reliable in Figure 3.14(a). The large separation of scales within the plume and the external regions is demonstrated here. The streamlines in the plume region clearly confirms the buoyant behavior that is observed in the flow visualization images, i.e. the plume always has a tendency to flow upwards over the building. In addition to visualizing flow structures, the PIV measurements are very useful for the validation of simulations using CFD codes.

Chapter 4: Conclusions

A quantitative salt-water modeling technique with particle image velocimetry diagnostic for analyzing the dispersion of a plume in a complex configuration was established in this study. The technique was validated by the good agreement of the results with previous studies using salt-water modeling with PLIF and LDV diagnostics, as well as with the turbulent point source plume theory. A crossflow generator was developed and the velocity profiles were characterized for four configurations. The dispersion of a plume under two different crossflow velocities is then studied using flow visualization and PIV techniques. The trajectories are compared with scaling laws and the classical correlations. Limited agreement has been found possibly due to non-uniformities in the crossflow velocity profile and vertical variations in the crossflow. Lastly, the dispersion of a plume in a crossflow near a building is analyzed. The trajectories of the plume near a building are compared with that in crossflow without a building, and the flow structures near the building are identified with PIV measurements. Overall, this study has established a salt-water technique for the study of accidental releases and the dispersion of hazardous materials in a complex configuration, and has demonstrated the capabilities on obtaining high fidelity quantitative and qualitative measurements of the flow dynamics. The specific results of each part of the study are summarized below, followed by the recommendations on future work.

Validation of Salt-Water Modeling with PIV Technique

- The whole velocity field measurements are obtained for flow rates of 110 ml/min (Case1) and 165 ml/min (Case 2) at salt mass concentration of 13%.

- Case 1 and Case 2 results agreed closely with theory both in terms of the (1/3) power law and the C_v constant. The results also showed good agreement with previous experiment results by Yao [43, 44, 45].

Development and Characterization of Crossflow Generator System

- A crossflow generator system is constructed comprising of a blower, four sump pumps, connecting pipes and the supporting structure. The system served as an add-on capability for the existing salt-water modeling facility.

- The velocity profile of the blower was characterized for four configurations, of which two were chosen to provide different crossflow velocities.

Dispersion of Plume in Crossflow

- The dispersions of a plume under two crossflow velocities were analyzed using the blue dye flow visualization and PIV techniques.

- Limited agreement was found between the trajectories of the plume, the classical Briggs plume rise equation and the scaling laws.

Dispersion of Plume in Crossflow near a Building

- The dispersions of a plume near a building under two crossflow velocities were analyzed using the blue dye flow visualization and PIV techniques.

- The presence of a building was found to push the plume trajectory back towards the source and upwards away from the building when compared with the trajectory of a plume in crossflow.

- Flow structures on the roof of the building and at the base of the building were shown using PIV measurements.

Future Work:

- A wide-angle lens may be used in place of the current lens so that a larger field of view can be obtained while maintaining a similar distance between the lens and the plume. This will allow the same intensity of particle illumination to reach the camera while allowing more of the plume to be "seen" by the lens.

- The velocity profile of the blower may be further improved by considering more configurations with the objective of further reducing the momentum of the incoming jets into the blower. Possible configurations include the use of pipes with equally spaced holes in the blower and the use of baffles to section the internal void of the blower.

- Flow structures of a plume in crossflow in the x_3-plane, such the bifurcation of the flow into two counter-rotating vortices, are known to be important. Methods to capture images in this plane in addition to the current x_2-plane may be explored, either using the existing or an additional set of laser and camera.

- The building should be introduced after a distance of x_3 / D=20 to isolate results from details of source and effects of source geometry. Ideally, the building should be located in the region where x_3 / D>40-50, corresponding to the self-similar region for the plume in crossflow.

- The dispersion of a plume in a crossflow near a building may be extended by carrying out experiments using different source strengths and varying the source distance as well as the building aspect ratio.

- A multiple source scenario may also be investigated for the classical unconfined plume and the plume in crossflow to determine the interaction between the flows and the mixing dynamics.

Bibliography

1. Sherlock, R.H. and Stalker, E.A., *The Control of Gases in the Wake of Smoke Stacks.* Mechanical Engineering*,* 1940. **52**: p. 455-458.

2. Hohenleiten, H.L. von and Wolf, E.F., *Wind-Tunnel Tests to Establish Stack Height for Riverside Generating Station*. Trans. ASME*,* 1942. **64**: p. 671-683.

3. Bryant, L.W., *The Effects of Velocity and Temperature of Discharge on the Shape of Smoke Plumes from a Funnel or Chimney in a Wind Tunnel*. National Physical Laboratory (Report ACSIL/49/2482), 1949. p. 1-28.

4. Strom, G.H. and Halitsky, J., *Important Considerations in the Use of the Wind Tunnel for Pollution Studies of Power Plants.* Air Repair, 1954. **4**(2): 25 pp. (Also Paper No. 54-SA-41, ASME Semi-Annual Meeting, Pittsburgh, Pa., June 20-24, 1954).

5. Halitsky, J., *Diffusion of Vented Gas Around Buildings*. J. Air Pollution Control Association, 1962. **12**(2): p. 74-80.

6. Halitsky, J., *Gas Diffusion Near Buildings.* Meteorology and Atomic energy, 1968. US Atomic Energy Commission TID-24190 Oak Ridge, TN Ch 5-5: p. 221-255.

7. Halitsky, J., *Validation of Scaling Procedures for Wind Tunnel Model Testing of Diffusion Near Buildings.* New York University, Dept. of Meteorology and Oceanography Tech. Report No. TR-69-8, 1969. p. 205.

8. Cermak, J.E., Sandborn, V.A., Plate, E.J., Binder, G.H., Chuang, H., Meroney, R.N., and Ito, S., *Simulation of Atmospheric Motion by Wind-tunnel Flows.* Civil Engineering Report CER66JEC-VAS-EJP-GJB-HC-RNM-SI17, Colorado State University Fort Collins, CO, 1966. p. 111.

9. Melbourne, W.H., *Wind Tunnel Modeling of Buoyant Chimney Plumes*. 3rd Australasian Conference on Hydraulics and Fluid Mechanics, The Institution of Engineers, Australia. 1968. Paper No. 2631 p. 81-85.

10. Snyder, W.H., *Similarity Criteria for the Application of Fluid Models to the Study of Air Pollution Meteorology*. Boundary-Layer Meteorology, 1972. **3**: p. 113-134.

11. Snyder, W.H., *Guideline for Fluid Modeling of Atmospheric Diffusion.* US Environmental Protection Agency Report EPA-600/8-81-009, 1981. p. 199.

12. Golden, J., *Scale Model Techniques.* M.Sc. Thesis, College of Engineering, 1961. New York University, New York, p. 48.

13. Castro, I.P. and Robins, A.G., *The flow around a surface-mounted cube in uniform and turbulent streams.* J. Fluid Mechanics, 1977. **79**(2): p. 307-335.

14. Snyder, W.H., *Some Observations of the Influence of Stratification on Diffusion in Building Wakes.* Institute of Mathematics and Its Applications, Meeting on Stably Stratified Flows. Sept. 21-23, 1992, U. of Surrey, Guildford, UK, p. 25.

15. Briggs, G.A., *A plume rise model compared with observations.* JAPCA, 1965. **15**: p. 433- 438.

16. Briggs, G.A., *CONCAWE meeting: discussion of the comparative consequences of different plume rise formulas.* Atmos. Envir., 1968. **2**: p. 228-232,

17. Slade, D.H., *Meteorology and Atomic energy.* US Atomic Energy Commission TID-24190 Oak Ridge, TN, 1968. p. 455.

18. Briggs, G.A., *Plume Rise*, USAEC Critical Review Series, 1969

19. Briggs, G.A., *Some recent analyses of plume rise observation*. Proc. Second Internat'l. Clean Air Congress, Academic Press, New York, 1971

20. Briggs, G.A., *Discussion: chimney plumes in neutral and stable surroundings*.

Atmos. Envir. 1972, **6**: p. 507-510.

21. Cermak, J.E., *Applications of Fluid Mechanics to Wind Engineering–A Freeman Scholar Lecture*. Journal of Fluids Engineering, 1974. **97**: p. 9-38.

22. Turner, J. S., Buoyant Plumes and Thermals., Annual Review of Fluid

Mechanics, 1969, **1**, pp. 29-44.

23. Turner, J. S., *Buoyancy Effects in Fluids*. Cambridge University Press, Cambridge, 1973.

24. Tennekes, H., and Lumley, J. L., *A First Course in Turbulence*, MIT Press, Cambridge, 1972. p. 113-124.

25. Hinze, J. O., *Turbulence*, 2nd ed. 1975, McGraw-Hill, New York, p. 534-584.

26. Chen, C. J., Rodi, W., *Vertical Turbulent Buoyant Jets: A Review of Experimental Data,* 1980. Pergamon Press. Oxford.

27. List, E. J., *Turbulent Jets and Plumes*, Ann. Rev. Fluid Mech., 1982. **14**, p. 189-212.

28. Morton, B. R., *Forced Plumes*, J. Fluid Mech., 1959. **5**, p. 151-163.

29. Middleton, J. H., *The Asymptotic Behavior of a Starting Plume.* J. Fluid Mech., 1975. **93**, p. 241-250.

30. Delichatsios, M. A., *Time Similarity Analysis of Unsteady Buoyant Plumes*. J. Fluid Mech., 1979. **93**, p. 241-250.

31. Anwar, H. O., *Experiment on an Effluent Discharging From a Slot Into Stationary or Slow Moving Fluid of Greater Density*. J. Hydraul. Res., 1969. **7**, p. 411-430.

32. Lutti, F. M., and Brzustowski, T. A., *Flow Due to a Two-Dimensional Heat Source With Cross Flow in the Atmosphere*. Combust. Sci. Technol., 1977. **16**: p. 71-87.

33. Andreopoulos, J., Heat Transfer Measurements in a Heated Jet-Pipe Flow Issuing Into a Cold Cross Stream. Phys. Fluids, 1977. **26**, p. 3200-3210.

34. Alton, B. W., Davidson, G. A., and Slawson, P. R., *Comparison of a Crossflow*. Atmos. Environ., 1993. Part A, **27A**, p. 589-598.

35. Baum, H. R., McGrattan, K. B., and Rehm, R. G., *Simulation of Smoke Plumes From Large Pool Fires*. Proceedings of the Combustion Institute, 1994. **25**: p. 1463-1469.

36. Quintiere, J.G., *Scaling Applications in Fire Research*. Fire Safety Journal, 1989. **15**: p. 3-29.

37. Heskestad, G., *Physical Modeling of Fire*. J. Fire and Flammability, 1975. **6**(7): p. 253-273.

38. Sangras, R., and Faeth, G.M., *Buoyant Turbulent Jets and Plumes: III. Round turbulent Nonbuoyant Starting Jets and Puffs and Buoyant Starting Plumes and Thermals.* Report No. GDL/GMF-99-03, 1999.

39. Steckler, K. D., Baum, H. R., and Quintiere, J. G., *Salt-water Modeling of Fire Induced Flows in Multi-compartment Enclosures.* Twenty-first Symposium (International) on Combustion, 1986: p. 143-149.

40. Kelly, A.A., *Examination of Smoke Movement in a Two-Story Compartment Using Salt Water and Computational Fluid Dynamics Modeling*, in *Fire Protection Engineering Department*. 2001, University of Maryland: College Park.

41. Clement, J.M., and Fleischman, C.M., *Experimental Verification of the Fire Dynamics Simulator Hydrodynamic Model.* Fire Safety Science - Proceedings of the Seven International Symposium, 2002: p. 839-851.

42. Jankiewicz, S.P., *Prediction Smoke Detector Response Using A Quantitative Salt-water Modeling Technique*, in *Fire Protection Engineering Department*. 2003, University of Maryland: College Park.

43. Yao, X., Ma, T., Marshall, A.W. and Trouve, A. *Mixing and Turbulent Transport in Unconfined and Impinging Plumes*. in *10th International Fire Science and Engineering Conference -InterFlam*. 2004. Edinburgh, Scotland.

44. Yao, X., and Marshall, A.W., *Quantitative Salt-water Modeling of Fire Induced Flow.* Fire Safety Journal, Oct 2006. 41(7): p. 497-508.

45. Yao, X., and Marshall, A.W. *Characterizing of Ceiling Jet Dynamics With Salt-water Modeling*. in *Fire Safety Science - Proceedings of the Eighth International Symposium, IAFSS*. 2005. Beijing, China.

46. McCaffrey, B.J., *Purely Buoyant diffusion Flames: Some Experimental Results.* Center For Fire Research, 1979.

47. Yao, X., 2006, *Characterization of Fire Induced Flow Transport Along Ceilings Using Salt-Water Modeling.* Dissertation for Ph.D, Dept of Fire Protection Engineering, University of Maryland.

48. Sangras, R., Kwon., O. C., and Faeth, G. M., *Self-Preserving Properties of Unsteady Round Nonbuoyant Turbulent Starting Jets and Puffs in Still Fluids.* ASME J. Heat Transfer, 2002. **124**, pp. 460-469.

49. Diez, F. J., Bernal, L. P., Faeth, G. M., *Round Turbulent Thermals, Puffs, Starting Plumes and Starting Jets in Uniform Crossflow*. Transactions of the ASME, 2003. **125**: p. 1046-1057

50. Zukoski, E. E., Kubota, T. and Cetegen, B., *Entrainment in Fire Plumes*, Fire Safety Journal, 1980/81. **3**: p. 107-121.

51. Zukoski, Z.Z., *Combustion Fundamentals of Fire*. 1995: Academic Press Ltd.

52. Heskestad, G., *Virtual Origins of Fire Plumes.* Fire Safety Journal, 1983. **5**: p. 109-114.